Paleoceanography and Paleoclimatology

AGU ADVANCING EARTH AND SPACE SCIENCES

RESEARCH ARTICLE
10.1029/2023PA004675

High-Resolution, Multiproxy Speleothem Record of the 8.2 ka Event From Mainland Southeast Asia

Christopher T. Wood[1,2], Kathleen R. Johnson[1], Lindsey. E. Lewis[1], Kevin Wright[1], Jessica K. Wang[1], Andrea Borsato[3], Michael L. Griffiths[4], Andrew Mason[5], Gideon M. Henderson[5], Jacob B. Setera[6,7], Silvia Frisia[3], Sengphone Keophanhya[8], and Joyce C. White[9,10]

[1]Department of Earth System Science, University of California, Irvine, CA, USA, [2]National Isotope Centre, GNS Science/Te Pū Ao, Lower Hutt, New Zealand, [3]School of Environmental and Life Sciences, University of Newcastle, NSW, Australia, [4]Department of Environmental Science, William Paterson University, Wayne, NJ, USA, [5]Department of Earth Sciences, University of Oxford, Oxford, UK, [6]Department of Earth and Planetary Sciences, Rutgers University, Piscataway, NJ, USA, [7]Now at CASSMAR, University of Texas at El Paso—Jacobs JETS II Contract, NASA Johnson Space Center, Houston, TX, USA, [8]Cultural Section, Department of Information, Culture and Tourism, Luang Prabang, LA, [9]Institute for Southeast Asian Archaeology, Philadelphia, PA, USA, [10]Department of Anthropology, University of Pennsylvania, Philadelphia, PA, USA

Key Points:

- High-resolution speleothem record of the 8.2 ka event in northern Laos shows weakened monsoon intensity and reduced local rainfall amounts
- Multiproxy data suggest the disruption to local rainfall amounts started decades before the weakened monsoon intensity inferred from $\delta^{18}O$
- Previous monsoon records of the event lack the resolution and/or multiproxy dimensions needed to reconstruct local hydrologic changes

Correspondence to:
C. T. Wood,
c.wood@gns.cri.nz

Citation:
Wood, C. T., Johnson, K. R., Lewis, L. E., Wright, K., Wang, J. K., Borsato, A., et al. (2023). High-resolution, multiproxy speleothem record of the 8.2 ka event from Mainland Southeast Asia. *Paleoceanography and Paleoclimatology*, *38*, e2023PA004675. https://doi.org/10.1029/2023PA004675

Received 22 MAY 2023
Accepted 1 NOV 2023

Abstract The 8.2 ka event is the most significant global climate anomaly of the Holocene epoch, but a lack of records from Mainland Southeast Asia (MSEA) currently limits our understanding of the spatial and temporal extent of the climate response. A newly developed speleothem record from Tham Doun Mai Cave, Northern Laos provides the first high-resolution record of this event in MSEA. Our multiproxy record ($\delta^{18}O$, $\delta^{13}C$, Mg/Ca, Sr/Ca, and petrographic data), anchored in time by 9 U-Th ages, reveals a significant reduction in local rainfall amount and weakening of the monsoon at the event onset at ~8.29 ± 0.03 ka BP. This response lasts for a minimum of ~170 years, similar to event length estimates from other speleothem $\delta^{18}O$ monsoon records. Interestingly, however, our $\delta^{13}C$ and Mg/Ca data, proxies for local hydrology, show that abrupt changes to local rainfall amounts began decades earlier (~70 years) than registered in the $\delta^{18}O$. Moreover, the $\delta^{13}C$ and Mg/Ca also show that reductions in rainfall continued for at least ~200 years longer than the weakening of the monsoon inferred from the $\delta^{18}O$. Our interpretations suggest that drier conditions brought on by the 8.2 ka event in MSEA were felt beyond the temporal boundaries defined by $\delta^{18}O$-inferred monsoon intensity, and an initial wet period (or precursor event) may have preceded the local drying. Most existing Asian Monsoon proxy records of the 8.2 ka event may lack the resolution and/or multiproxy information necessary to establish local and regional hydrological sensitivity to abrupt climate change.

Plain Language Summary The most significant global climate event in the last ~11,000 years occurred ~8,200 years ago (the "8.2 ka event"). Many globally distributed records of past climate (paleoclimate) document significant changes during the event, but there are few from Mainland Southeast Asia available to reconstruct the climate impacts in this region. We present a new speleothem (cave sample) record from Tham Doun Mai Cave, Northern Laos that uses multiple geochemical and physical signals (proxies) to document local and regional climate effects of the 8.2 ka event at a high resolution. Using oxygen isotopes, we find that the 8.2 ka event weakened regional monsoon intensity for at least ~170 years, which resembles findings from other studies. However, other proxies suggest local rainfall changed abruptly decades before the signal of monsoon weakening. Additionally, local drying may have lasted much longer than current estimates of 8.2 ka event responses. Most proxy records of the 8.2 ka event in monsoon regions lack similar multiproxy information and/or do not have high enough resolution to fully capture the climatic response. Additional records like ours from monsoon regions may assist in establishing how sensitive local and regional rainfall is to abrupt climate change.

1. Introduction

A significant global climate anomaly that began around 8.2 ka BP (thousand years before present, where present is 1950 CE), commonly referred to as the "8.2 ka event," caused abrupt climatic changes lasting for at least ~160–170 years as evidenced by numerous proxy records from several continents (Alley et al., 1997; Kobashi et al., 2007). This event, which is likely the most significant of the Holocene Epoch, has been attributed to

10.1029/2023PA004675

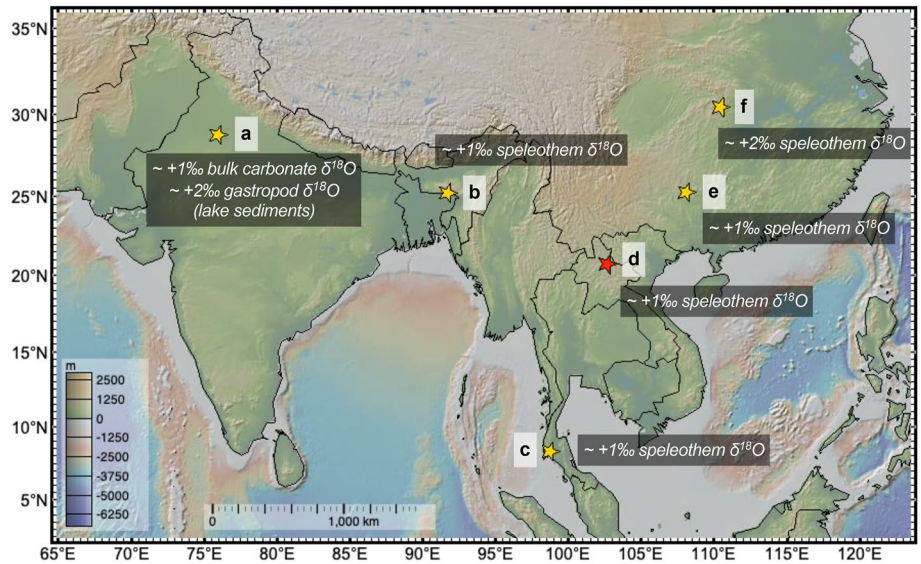

Figure 1. Locations of selected proxy records (red star (d), this study; yellow stars, previous studies) that show hydroclimate responses to the 8.2 ka event in the Asian Monsoon domain. (a) Lake Riwasa, NW India (Dixit et al., 2014); (b) Mawmluh Cave, NE India (Berkelhammer et al., 2012); (c) Klang Cave, S Thailand (Chawchai et al., 2021); (d) Tham Doun Mai Cave, N Laos (this study); (e) Dongge Cave, China (Cheng, Fleitmann, et al., 2009); (f) Heshang Cave, China (Y. H. Liu, et al., 2013; Owen et al., 2016). Individual studies from these locations suggest a weakened monsoon and/or relatively dry conditions in response to the event. Positive shifts in $\delta^{18}O$ are labeled in figure. Figure made utilizing GeoMapApp (www.geomapapp.org)/CC BY/CC BY (Ryan et al., 2009).

freshwater input into the North Atlantic from a glacial outburst flood or ice sheet saddle collapse in the final stages of deglaciation (Alley & Ágústsdóttir, 2005; Cheng, Edwards, et al., 2009; Matero et al., 2017). Numerous effects in the North Atlantic and surrounding areas are well documented (e.g., Kleiven et al., 2008; Morrill & Jacobsen, 2005), but the spatial fingerprint of the event continues to be discovered and refined. Proxy records with robust age models suggest that climate teleconnections created varying responses to a singular event, including temperature anomalies interpreted from Greenland ice cores (Thomas et al., 2007), shifts in mid-latitude monsoon systems (Cheng, Fleitmann, et al., 2009; Y. H. Liu et al., 2013), and alterations of storm tracks and rainfall amounts in western North America (de Wet et al., 2021; Johnson, 2021a; Oster et al., 2017).

Sedimentary archives from numerous regions suggest that the meltwater event caused a weakening of the Atlantic Meridional Overturning Circulation (AMOC) and southward shift of the global Intertropical Convergence Zone (ITCZ) during the 8.2 ka event (Cheng, Fleitmann, et al., 2009; Duan et al., 2021; Ljung et al., 2008; Morrill & Jacobsen, 2005; Peros et al., 2017; Voarintsoa et al., 2019). Speleothem records from China suggest a weakening of the Asian Monsoon system in response to these changes (Cheng, Fleitmann, et al., 2009; Duan et al., 2023; Y. J. Liu et al., 2013; Morrill et al., 2011), but potential spatial variability across the monsoon regions of South and Southeast Asia is not well defined. In the East Asian Summer Monsoon (EASM) region, a speleothem record from Heshang Cave (Figure 1f) indicates that monsoon weakening was synchronous with abrupt cooling in Greenland at 8.25 ± 0.10 ka BP, suggesting a rapid atmospheric teleconnection between the North Atlantic and the EASM (Y. H. Liu et al., 2013). A recent stalagmite record from North China (Duan et al., 2023) further supports this interpretation, and identifies three weak monsoon excursions within the 8.2 ka event that are coherent with Greenland temperature history. Lake and speleothem proxy records from northern India (Figure 1a) indicate the Indian Summer Monsoon (ISM) weakened across the event, although the 8.2 ka event response recorded in speleothem $\delta^{18}O$ in northeast India is less striking than other Holocene changes (Berkelhammer et al., 2012; Dixit et al., 2014; Walker et al., 2018). Similarly, terrestrial proxy records of the event in southern India show a subdued response to the 8.2 ka event, indicating this region may not be as affected by changes to the ITCZ (Banerji et al., 2020). In Mainland Southeast Asia (MSEA), dry conditions have been observed through the 8.2 ka event in at least one record from southern Thailand (Figure 1c) (Chawchai et al., 2021). However, the composite speleothem $\delta^{18}O$ anomaly in Chawchai et al. (2021) is small compared with other $\delta^{18}O$ shifts recorded by the same speleothem. Additionally, proxy records from Thailand and Cambodia show contrasting hydroclimate

responses during the event (Chabangborn et al., 2020; Chawchai et al., 2013; Maxwell, 2001). Therefore, because no high-resolution records of the 8.2 ka event currently exist in MSEA—a critical region linking the ISM and EASM—we lack knowledge in the sensitivity of rainfall patterns across MSEA in response to abrupt climate change.

Speleothem records frequently contain multiple environmentally sensitive proxies and offer U-Th age models with low uncertainties, making them ideal for investigating centennial-scale climate anomalies such as the 8.2 ka event (Feinberg & Johnson, 2021; Wendt et al., 2021). Prior work has shown the utility of using multiple speleothem proxies to infer environmental changes through the 8.2 ka event (Allan et al., 2018; de Wet et al., 2021; Y. H. Liu et al., 2013; Oster et al., 2017; Owen et al., 2016; Waltgenbach et al., 2020), particularly in light of recent research highlighting the advantage of additional proxies such as trace elements, calcite fabric, and optical fluorescence in interpreting the $\delta^{18}O$ time series (Faraji et al., 2022; Griffiths et al., 2020; Johnson, 2021a, 2021b; Patterson et al., 2023; Vanghi et al., 2018, 2019; Wright et al., 2023; Zhang et al., 2018).

Most speleothem records documenting monsoon changes during the 8.2 ka event rely solely on $\delta^{18}O$ (Chawchai et al., 2021; Dong et al., 2010; Duan et al., 2023; Dykoski et al., 2005; Y. J. Wang et al., 2005). While not completely decoupled from local rainfall amounts, interpretation of Asian Monsoon speleothem $\delta^{18}O$ relies on a significant upstream rainout control (Chiang et al., 2015; Dayem et al., 2010; Johnson, 2011; Pausata et al., 2011; Yuan et al., 2004), and a more positive $\delta^{18}O$ signal is generally indicative of a regionally weakened monsoon state (Cheng et al., 2016; Y. J. Wang et al., 2001; Yang et al., 2016). As a result, we still lack a complete understanding of the local/regional hydroclimate response to abrupt climate events of the deglaciation and Holocene in the Asian monsoon region. There is a notable exception to this, however, which is the multiproxy reconstructions from Heshang Cave (Figure 1f) (Y. H. Liu et al., 2013; Owen et al., 2016) in central China. Specifically, Y. H. Liu et al. (2013) utilized Mg/Ca to extend their interpretation of $\delta^{18}O$ controls and the full response to include changes in rainfall amounts, while Owen et al. (2016) provided a semi-quantitative method for estimating changes in rainfall amount using $^{44}Ca/^{42}Ca$ measurements. Additional speleothem records incorporating multiple geochemical proxies that represent a more "local" signal of past hydrology are required to more confidently reconstruct changes in Asian Monsoon rainfall amounts, particularly across MSEA, during the 8.2 ka event.

Here we present a new high-resolution multiproxy record of the 8.2 ka event period (~8.9–7.6 ka BP) from a precisely dated stalagmite (TM-17) from Tham Doun Mai Cave (TDM), Northern Laos (Figure 1d). Our record is based on high-resolution stable isotope ($\delta^{18}O$ and $\delta^{13}C$) and trace element (Mg/Ca and Sr/Ca) measurements, synchrotron radiation micro-X-ray fluorescence (SR-μXRF), as well as optical and fluorescent light microscopy, which allow us to examine the climatic response of MSEA hydroclimate to the 8.2 ka event.

2. Materials and Methods

Speleothem TM-17 from TDM cave, Northern Laos (Figure 1d; 20°45′N, 102°39′E; 352 m asl), is a ~60 cm candle-shaped stalagmite. TDM cave, a roughly 3.75 km solution cave within Carboniferous-Permian aged limestones, is ~30 m above the Nam Ou River in Nong Khiaw District, Luang Prabang Province, Laos (Dreybrodt et al., 2013; Kiernan, 2015). TDM experiences ~1,195 mm of annual precipitation with the majority during the June–September summer monsoon season, and moisture source regions are traced to the Indian Ocean and Bay of Bengal (Yang et al., 2016). Influences on stalagmite $\delta^{18}O$ are linked to upstream rainout, and local precipitation $\delta^{18}O$ is also influenced by the El Niño-Southern Oscillation (Griffiths et al., 2020; J. K. Wang et al., 2019; Yang et al., 2016). The top section of stalagmite TM-17 was previously analyzed for a high-resolution stable isotope analysis of the Common Era (last 2 ka BP) (J. K. Wang et al., 2019). TM-17 was collected ~200 m from the TDM cave entrance (J. K. Wang et al., 2019) on a steep, nearly vertical slope that precedes a vertical drop-off of ~20 m to the river level/water table below. Therefore, we estimate TM-17 was situated under at least 100 m of epikarst or bedrock based on topographic maps of the area, and parts of the cave may be under ~400 m of bedrock (Dreybrodt & Laumanns, 2013). This is in contrast to stalagmites from TDM utilized in Griffiths et al. (2020), which were collected in a corridor closer to the cave entrance, where bedrock thickness is likely closer to ~20 m.

For high-resolution analyses of the 8.2 ka section of the stalagmite, a ~7.40 cm long slab of TM-17 was cut from a polished half of the stalagmite for microsampling and laser ablation ICPMS (LA-ICPMS) analysis (Figure 2). The central 3.13 cm section (depth from top of stalagmite = 19.92–16.79 cm) was micromilled for high-resolution sampling of calcite powder using a New Wave Instruments Micromill fitted with a diamond drill bit. Seven

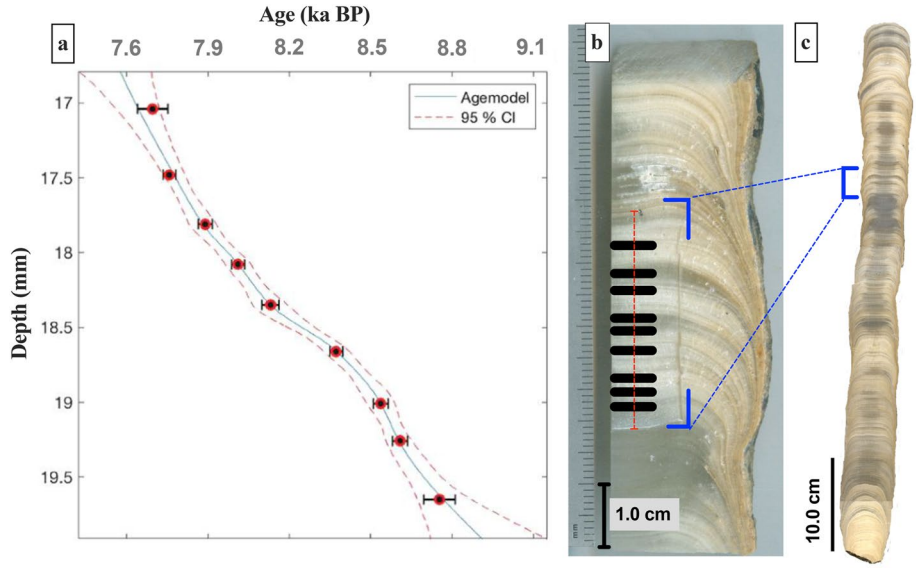

Figure 2. Age model and TM-17 stalagmite. (a) Age model for the 8.2 section of TM-17 used in this study developed using COPRA (Breitenbach et al., 2012). Circles represent mean modeled values for U/Th sampling depths bracketed by errors, and lines show likely values (solid line) and 95% confidence interval for age model (dashed lines). (b) Scan of sectioned TM-17 stalagmite piece (~21.7–14.3 cm from top) used for high-resolution micro-milling (stable isotopes; within blue brackets) and laser ablation inductively coupled plasma mass spectrometry for trace elements (red dashed line). Locations of midpoints for drilled U-Th measurement depths are represented as black horizontal shapes along vertical dashed line. (c) Full scan of TM-17 stalagmite following sawing and polishing (~60 cm in total length).

hundred stable isotope samples were milled at a resolution of 45 μm over the 3.13 cm section. Powders were analyzed for $\delta^{18}O$ and $\delta^{13}C$ composition using a Thermo Finnigan Kiel IV carbonate device coupled with a Delta V Plus isotope ratio mass spectrometer at the University of California, Irvine. Every sample was analyzed in the central portion of the section between depths 17.50–19.02 cm, while every second drilled sample was analyzed from outside depths (16.79–17.50 and 19.02–19.91), resulting in a 513-point sample set. Stable isotope results are expressed relative to the VPDB standard using conventional δ notation. Fifteen standards were analyzed with each batch of 31 stalagmite powders (IAEA-CO-1; NBS-18; and OX, an in-house quality control standard). The standard deviations (1σ) for stable isotopes in analyzed standards during all runs were 0.07‰ for $\delta^{18}O$ and 0.05‰ for $\delta^{13}C$.

Trace elements were analyzed in the same section of TM-17 by LA-ICPMS at Rutgers University using a Photon Machines Analyte Excite 193 nm excimer laser attached to a ThermoScientific iCAP-Q ICPMS. The instruments were tuned to limit fractionation and oxide production by ablating NIST612 glass for Th/U = 1 and ThO/Th < 0.4. Analyses were conducted along the trench created during high-resolution micro-milling for stable isotopes (Figure 2). Sample depths (distance from top of the stalagmite) were measured along the central growth axis, and depths were kept constant along visible growth layers perpendicular to this edge for the laser ablation sampling depths. Analyses consisted of rastered lines ablated at a speed of 5 μm/s using a spot size of 85 μm, a shot frequency of 10 Hz, and a fluence of 6.0 J/cm^2. Ablated material was carried to the plasma using a He carrier gas flow rate of 0.8 LPM. To remove surface contamination, areas of analyses were pre-ablated by the laser prior to main data acquisition runs. Isotopes ^{26}Mg, ^{29}Si, ^{31}P, ^{34}S, ^{55}Mn, ^{57}Fe, ^{63}Cu, ^{64}Zn, ^{88}Sr, ^{137}Ba, ^{138}Ba, and ^{238}U were monitored with 10 ms dwell times. Combined with the raster speed, a single pass over the entire mass range covered ~0.75 μm of sample. NIST glass 612 was used as the primary calibration standard and was analyzed frequently throughout the run to account for drift. Background subtraction, drift correction, and calibration were undertaken using the IGOR-based Iolite software (Paton et al., 2011).

SR-μXRF microscopy was performed on polished stalagmite samples at the XFM hard X-ray beamline at the Australian Synchrotron equipped with a Maia 384 detector array mounted 10 mm away from the sample target. The monochromatic incident energy was set at 18.5 keV, the beam spot size was 1.5 μm, with a pixel resolution of 4 × 4 μm. The energy range of the Australian Synchrotron XFM beamline (4–27 keV) is not suitable to detect

Table 1
TM-17 U-Th Results

Sample ID	Depth from top (cm)	^{238}U (ppm)	^{232}Th (ppb)	(^{234}U/^{238}U)	(^{230}Th/^{232}Th)	(^{230}Th/^{238}U)	(^{234}U/^{238}U)$_{initial}$	Raw age (years BP)	Corr. age (years BP)
TM-17-U9	17.04	3.35	1.00	1.6488 ± 0.0053	1,170.7 ± 18.8	0.1138 ± 0.0008	1.6630 ± 0.0054	7,703 ± 56	7,696 ± 56
TM17_8.2_U2	17.48	3.91	0.83	1.6636 ± 0.0056	1,670.7 ± 11.3	0.1158 ± 0.0003	1.6781 ± 0.0054	7,763 ± 23	7,758 ± 23
TM17_8.2_U3	17.81	3.30	1.58	1.6455 ± 0.0054	744.3 ± 4.2	0.1165 ± 0.0003	1.6599 ± 0.0054	7,901 ± 23	7,890 ± 26
TM17_8.2_U4	18.08	3.75	0.83	1.6539 ± 0.0055	1,636.6 ± 11.2	0.1187 ± 0.0003	1.6686 ± 0.0054	8,016 ± 24	8,011 ± 24
TM17_8.2_U5	18.35	3.07	3.21	1.6647 ± 0.0056	355.5 ± 1.8	0.1215 ± 0.0003	1.6800 ± 0.0054	8,154 ± 23	8,131 ± 32
TM17_8.2_U6	18.66	4.19	0.54	1.5988 ± 0.0054	2,855.4 ± 23.0	0.1197 ± 0.0003	1.6130 ± 0.0053	8,376 ± 23	8,373 ± 24
TM17_8.2_U7	19.01	4.05	2.14	1.5884 ± 0.0055	700.9 ± 3.4	0.1212 ± 0.0003	1.6026 ± 0.0052	8,550 ± 24	8,537 ± 27
TM17_8.2_U8	19.26	3.47	2.52	1.5857 ± 0.0053	513.5 ± 2.8	0.1221 ± 0.0003	1.5999 ± 0.0052	8,626 ± 22	8,609 ± 28
TM-17-U10	19.65	4.11	0.83	1.5804 ± 0.0050	1,868.0 ± 32.9	0.1234 ± 0.0008	1.5949 ± 0.0051	8,759 ± 57	8,754 ± 58

Note. Uncertainties are 2σ. Half lives are those of Cheng et al. (2013). All ages are relative to 1950. Corrected ages assume an initial ^{230}Th/^{232}Th atomic ratio of $5.38 + 5.38/-4.84 \times 10^{-6}$.

low Z elements such as Mg, Si, S, and P, and elements with a concentration below 1 ppm (Borsato et al., 2021), therefore, the elements detected were only Ca, Sr, Fe, and Zn. The XFM spectral data were analyzed using the GeoPIXE software suite, quantified by using single element Mn, Fe, and Pt foils (Micromatter, Canada) and matrix-corrected against Ca concentration (Borsato et al., 2021). Line scans were extracted with ImageJ on two parallel lines perpendicular to the growth direction by using a 20-pixel window (80 μm wide).

Petrographic thin sections (30 μm thick) were imaged using a Zeiss Axioplan microscope in plane-polarized light at the University of Newcastle, and their fabrics were described following the criteria illustrated in Frisia (2015). Fluorescent light images of thin sections, stimulated by 470 nm wavelength lasers, were obtained using a Zeiss Axio Imager A1 fluorescence microscope with an LED Colibri controller at the University of Newcastle, Australia. SR-μXRF, optical microscopy, and fluorescence were performed on a separate half of the TM-17 stalagmite versus LA-ICPMS and stable isotope sampling, and depths were measured independently.

The TM-17 age model is constrained by 9 U-Th dates spanning the 8.2 ka event (Figure 2; Table 1). U-Th samples were drilled using a Dremel tool and a diamond dental bur to attain ~200 mg of calcite powder. U-Th was then analyzed using multi-collector ICPMS (MC-ICPMS) at the University of Oxford, UK utilizing previously outlined methods (Hu et al., 2008; Mason & Henderson, 2010; J. K. Wang et al., 2019). Corrected ages (Table 1) assume an initial ^{230}Th/^{232}Th atomic ratio of 5.38 (+5.38/−4.84) × 10^{-6}, and the half-lives reported in Cheng et al. (2013). The age model was constructed using COPRA (Breitenbach et al., 2012), which calculates depth to age relationships between U-Th sampling points based on a Monte Carlo modeling approach (Figure 2).

3. Results

The TM-17 U-Th ages (n = 9) display uncertainties of ±24–58 years (Table 1), with a mean value of 30 years, which is our stated uncertainty for all chronology in the text. The COPRA age model extends from 8.91 to 7.58 ka BP (Figure 2). δ^{18}O values vary from −10.52 to −8.84‰ VPDB with a mean value of −9.84‰, and δ^{13}C varies from −7.39 to −3.64‰ VPDB with a mean value of −5.33‰ (Figures 3a and 3b). The mean sample resolution for δ^{18}O and δ^{13}C ranges from ~1 to 3 years, depending on the growth rate, which varies from ~13 to 71 μm/year with a mean of 24 μm/year (Figure 3d). LA-ICPMS analysis of trace elements resulted in mean values of 49.90 mmol/mol for Mg/Ca and 0.41 mmol/mol for Sr/Ca over the full time series (Figures 3 and 4). The 513 pt. age model used for stable isotopes was interpolated to the trace element LA-ICPMS data points at corresponding depths (41,993 points).

All proxies show anomalous shifts around the time of the 8.2 ka event (between ~8.4 and 8.1 ka BP), including more positive δ^{18}O, generally more negative δ^{13}C (with swings in both directions), and fluctuations in both Mg/Ca and Sr/Ca (Figures 3 and 4). For each proxy, values from ~8.91 to 8.40 ka BP were averaged ("pre-event average") to calculate 2σ excursions from the pre-event average. For δ^{18}O, the pre-event aver-

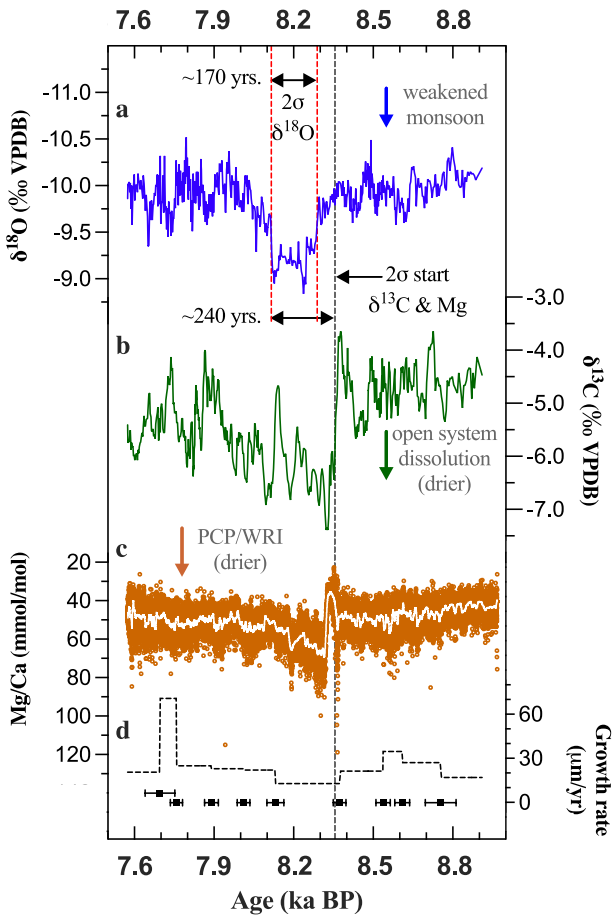

Figure 3. TM-17 multiproxy data for the 8.2 ka event range. (a, b) Five hundred thirteen pt. stable isotope records ($\delta^{18}O$ and $\delta^{13}C$); (c) laser ablation inductively coupled plasma mass spectrometry Mg/Ca data (central white line represents 100 pt running mean). (d) Growth rate estimates (dashed black line) calculated using U-Th ages; U-Th results represented by squares with brackets covering error range. Vertical dashed lines represent proxy anomalies (2σ) from the calculated pre-event average (~8.91–8.40 ka BP). See the text for full discussion of proxy interpretations and event length estimates.

age is −9.96‰ VPDB, and a positive anomaly greater than 2σ appears between 8.29 and 8.12 ka BP for a length of ~170 years. The maximum $\delta^{18}O$ value of TM-17 during the event is −8.84‰, a difference of 1.12‰ from the pre-event average, and the mean value during the anomaly is −9.20‰, a 0.76‰ difference from the pre-event period. Anomalous points (2σ or greater) outside of this continuous range occur outside of the event period on either side; if these are included, the anomaly in $\delta^{18}O$ can be extended to ~8.34–8.05 ka BP, for a maximum $\delta^{18}O$-based event duration of ~290 years.

The pre-event average in $\delta^{13}C$ is −4.76‰ VPDB, and a sharp decrease occurs prior to the 2σ $\delta^{18}O$ anomaly (Figure 3). The $\delta^{13}C$ data reaches 2σ from the pre-event average at ~8.36 ka BP, and the most negative value during the event is −7.39‰, a difference of 2.63‰ from the pre-event average. Large variations occur in the $\delta^{13}C$ data around the central and late stages of the event (within the $\delta^{18}O$ anomaly), so there is not a continuous 2σ excursion in $\delta^{13}C$ that approaches the length of the anomaly in $\delta^{18}O$. Additionally, $\delta^{13}C$ exceeds the pre-event average (more positive values) during the event period with a maximum of −4.67‰ at ~8.14 ka BP. Discontinuous anomalies (2σ) occur from 8.36 to 7.94 ka BP for a length of ~420 years.

Mg/Ca data display the highest values (maximum of 118.8 mmol/mol) at the onset of the Mg/Ca anomaly, though this excursion is too brief to appear in the smoothed curve (Figure 3). This is followed by a sharp decrease that reaches 2σ (<40.6 mmol/mol) from the pre-event average (47.4 mmol/mol) in close alignment with the $\delta^{13}C$ anomaly at ~8.36 ka BP. This decrease then abruptly reverses at ~8.32 ka BP, becoming more positive (>54.2 mmol/mol) than the pre-event average for the next ~150 years, and returning to lower values around 8.18 ka BP. Interestingly, this return to lower Mg/Ca values occurs prior to the negative rebound in $\delta^{18}O$ at the termination of the 8.2 ka event, and a discontinuous but steady sequence of anomalous values in Mg/Ca continues up to ~8.13 ka BP, for a total event duration length estimate of ~220 years. Further discontinuous Mg/Ca anomalies continue similarly to the full range of discontinuous $\delta^{13}C$ anomalies (>400 years). Positive anomalies after longer breaks in continuity occur for the rest of the Mg/Ca and $\delta^{13}C$ record, suggesting there is no complete return to stable values matching the pre-event averages (Figure 3).

Sr/Ca LA-ICPMS data show some structural similarities to the Mg/Ca record including anomalous values at the event initiation, and there is correlation between the data sets ($R^2 = 0.32$ or 0.41 for raw or smoothed data respectively; Figure 4). Synchrotron Sr/Ca reasonably matches LA-ICPMS Sr/Ca, although it more closely resembles LA-ICPMS Mg/Ca (Figure 4). This is in part related to the "edge effect," which tends to overestimate both negative and positive peaks in the SR-μXRF maps in correspondence with abrupt changes in the elemental concentration (Borsato et al., 2021). On the other hand, the flatter peaks in the LA-ICPMS Sr/Ca scan with respect to the synchrotron Sr/Ca data are also related to the coarser sampling (spot size of 85 μm) which result in a smoothing of the original signal. Unfortunately, the energy range of the Australian Synchrotron XFM beamline (4–27 keV) is not suitable to detect low Z elements such as Mg, and a direct comparison with the Mg/Ca LA-ICPMS is not possible. Decreased values of Sr/Ca are in line with the initial decadal shifts in Mg/Ca, and values increase similarly to Mg/Ca following the initial disruption by ~8.330 ka BP in our age model. Additionally, SR-μXRF scanning displays two prominent bands in Sr concentration that align with spikes of decreased Sr/Ca (Figures 5b and 5c). These two bands are matched in depth by two bands of increased fluorescence as seen in TM-17 thin sections (Figure 5a).

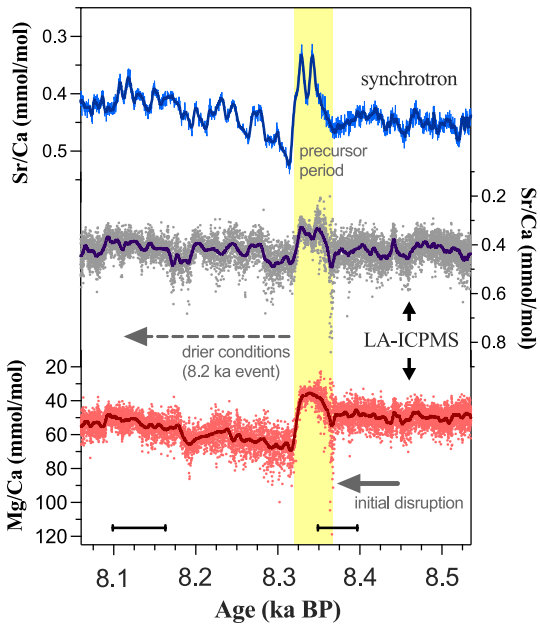

Figure 4. Sr/Ca from synchrotron and laser ablation inductively coupled plasma mass spectrometry (LA-ICPMS) compared to LA-ICPMS Mg/Ca over the event period. Synchrotron Sr/Ca (top) fit to the TM-17 age model (mmol/mol; heavy line is 11-pt smoothing of the average from two parallel line scans) for comparison to Mg/Ca and Sr/Ca LA-ICPMS data (mmol/mol; heavy lines are 100-pt mean). Synchrotron Sr/Ca more closely resembles LA-ICPMS Mg/Ca (vs. LA-ICPMS Sr/Ca) during the precursor period and 8.2 ka event period. Yellow shading indicates the anomalous precursor period before the sustained 8.2 ka event response. Error range of U-Th results from this section of the age model is represented by brackets at bottom of figure.

4. Discussion

4.1. TM-17 Proxy Interpretations at the 8.2 ka Event

For the TDM study site, Yang et al. (2016) found that correlations between local rainfall $\delta^{18}O$ and both sea level pressure and vertical wind shear in the Bay of Bengal suggest an upstream rainout control on local $\delta^{18}O$, with little influence from local precipitation amount. Hence, similar to previous work involving TDM, we interpret the positive anomaly at the 8.2 ka event in TM-17 $\delta^{18}O$ as evidence of a weakened monsoon intensity via less upstream rainout (Figures 3 and 5) (Griffiths et al., 2020; J. K. Wang et al., 2019). The homogenous positive $\delta^{18}O$ excursions between northern Laos and EASM sites across eastern China (Figures 1 and 5), interpreted as a general weakening of the monsoon and/or locally dry conditions (Cheng, Fleitmann, et al., 2009; Dykoski et al., 2005; Hu et al., 2008; Y. H. Liu et al., 2013), indicate a regionally coherent response across much of the EASM domain. Higher $\delta^{18}O$ values are also observed in EASM speleothem records during millennial-scale Northern Hemisphere cooling events such as Heinrich Stadials and the Younger Dryas (Cheng et al., 2016). These longer, millennial-scale events are thought to be caused by similar climatic forcings to the 8.2 ka event, namely a North Atlantic fresh water forcing creating a weakening of the AMOC (Alley & Ágústsdóttir, 2005; McManus et al., 2004).

The $\delta^{18}O$ anomalies during the 8.2 ka event in Dongge Cave (Dykoski et al., 2005; updated age model in Cheng, Fleitmann, et al., 2009) and Heshang Cave (Y. H. Liu et al., 2013) are the most comparable for assessing a regional signal in TM-17 $\delta^{18}O$ (Figures 1d–1f). The maximum $\delta^{18}O$ value at Heshang Cave is 2.15‰ more positive than its pre-event average (Figure 6), while the $\delta^{18}O$ increase from the pre-event average in stalagmite D4 from Dongge Cave is 1.31‰. The highest anomaly in TM-17 $\delta^{18}O$ during the 8.2 ka event is 1.12‰ above the pre-event average (Figures 3 and 5). The ~1‰ difference in magnitude between Heshang (2.15‰) versus Dongge and TDM (1.31‰ and 1.12‰, respectively) may be due to regional differences in the $\delta^{18}O$ of precipitation and/or local environmental or hydrologic controls that affect stalagmite $\delta^{18}O$. For instance, spatial variability in temperature, moisture recycling, or upstream rainout responses during the 8.2 ka event could lead to different magnitude $\delta^{18}O$ shifts in speleothem $\delta^{18}O$ at the different cave sites (Hu et al., 2008; G. Liu et al., 2020). Furthermore, locally specific karst hydrologic effects could create discrepancies in speleothem $\delta^{18}O$ responses at different drip sites within and between different caves (Bradley et al., 2010; Treble et al., 2022).

Mg/Ca and Sr/Ca are often linked to above-cave hydrologic changes through prior calcite precipitation (PCP) and water-rock interaction (WRI), both of which will increase these trace elements relative to Ca during dry periods (Fairchild et al., 2006; Sinclair et al., 2012). An indication of hydrologic control on Mg/Ca and Sr/Ca is correlation between the two proxies (Fairchild & Treble, 2009; Johnson et al., 2006; Tremaine & Froelich, 2013). Mg/Ca and Sr/Ca in TM-17 LA-ICPMS data correlate ($R^2 = 0.32$), suggesting hydrologic influence. A 100-point smoothing of Mg/Ca and Sr/Ca data results in a correlation of $R^2 = 0.41$. Therefore, we interpret Mg/Ca to be representative of a PCP and WRI control that increases Mg/Ca during dry periods, and we interpret the increased Mg/Ca during the 8.2 ka event to represent local drying (Figure 3). While there is not a sustained increase in LA-ICPMS Sr/Ca for the length of the 8.2 ka event, synchrotron Sr/Ca resembles Mg/Ca data and displays both the precursor period of decreased values and the increased Sr/Ca during the following event period (Figure 4). In addition to the "edge effect" (Borsato et al., 2021) potentially affecting synchrotron data, it is likely that variable patterns of growth bands on TM-17 resulted in LA-ICPMS lines missing some of the stronger shifts in Sr/Ca that are apparent in synchrotron data (Figure 5).

TM-17 Mg/Ca displays several of the highest individual values of the record (>2σ from the pre-event average, but too brief to appear in the smoothed curve) at ~8.36 ± 0.03 ka BP, suggesting an abrupt onset of drought conditions readily explained by PCP and WRI controls (Figure 3). Mg/Ca then decreases briefly for ~30 years, a pattern mirrored in Sr/Ca from LA-ICPMS and synchrotron data sets (Figures 4 and 5). Clear bands of both

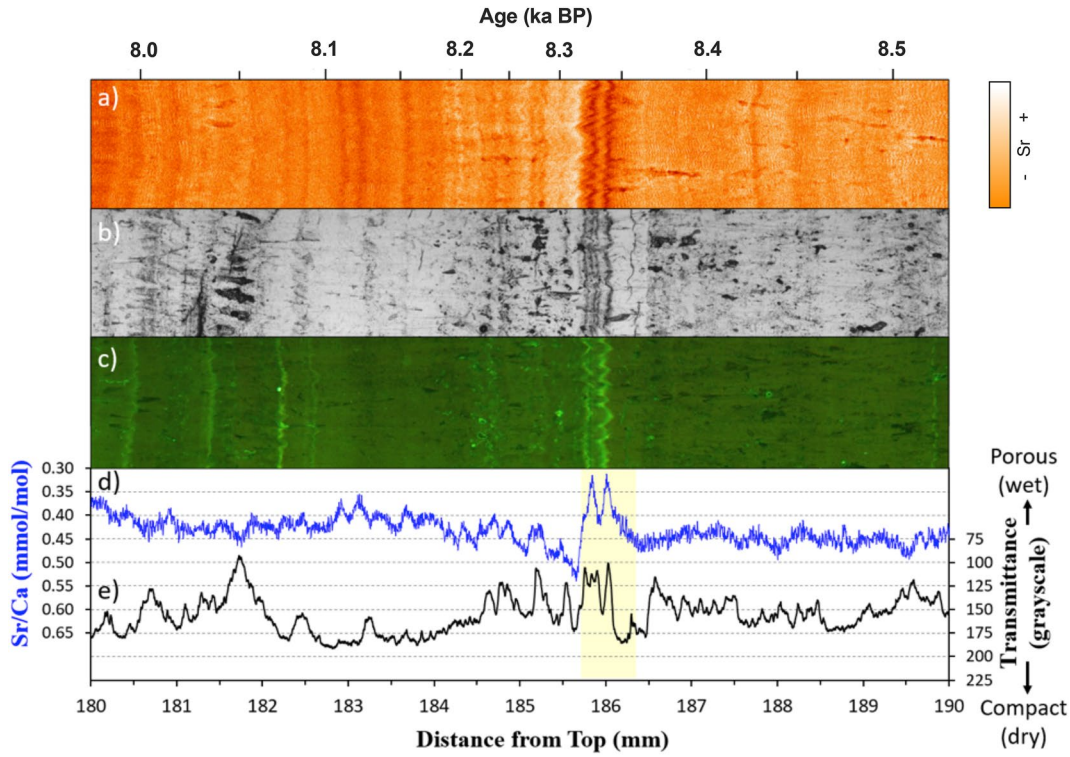

Figure 5. Synchrotron radiation micro-X-ray fluorescence (SR-μXRF) and petrography data for TM-17 plotted versus distance from top of the stalagmite. (a) Strontium SR-μXRF map (red temperature scale) where dark red color corresponds to low concentration and light-red to white color corresponds to high concentration; (b) thin section transmitted light optical microscopy image; (c) thin sections fluorescent light (470 nm wavelength) image; (d) synchrotron Sr/Ca (mmol/mol) concentration extracted from the above image (a) as averaged values along two 80 μm wide traverses; and (e) transmittance profile extracted from the above optical microscopy image (b) along a 1 mm wide window (250 pixels) and reported as grayscale values where a value of 0 corresponds to black and 255 corresponds to white. Higher grayscale values correspond to translucent calcite layers (compact columnar fabric) indicative of constant slow drip rate (dry periods), whereas lower values are associated with opaque calcite layers (porous fabric) indicative of higher, variable drip rate (wet periods). The yellow band highlights the position of the "precursor period" characterized by a twin band with the lowest Sr values and the highest fluorescence and micro-porosity values in the entire studied section.

low Sr (SR-μXRF) and increased fluorescence are visible in TM-17 imaging and coincide with decreased Sr/Ca in synchrotron line data during this period (Figures 4 and 5). LA-ICPMS Mg/Ca and Sr/Ca decreases support this interpretation, suggesting this precursor period may have had higher than average rainfall amounts following the initial disruption seen in Mg/Ca (Figure 4). After this period, a sustained increase of Mg/Ca relative to the pre-event average defines the response for the majority of the event period. This sustained increase is matched in synchrotron Sr/Ca (Figures 4 and 5). The highest values of the smoothed Mg/Ca data during this sustained increase occur at ~8.32 ka BP, which matches the onset of the event in $\delta^{18}O$ (Figure 3).

In contrast with $\delta^{18}O$, TM-17 $\delta^{13}C$ is likely more responsive to the local water balance at TDM, as previously demonstrated for two Holocene speleothem records from this site (Griffiths et al., 2020; J. K. Wang et al., 2019). However, multiple controls on $\delta^{13}C$ are potentially active, and interpretations of this proxy may vary depending on the cave setting and time period (Johnson, 2021b; Wong & Breecker, 2015). Previous studies have attributed control of speleothem $\delta^{13}C$ to soil respiration (Genty et al., 2001), vegetation density and/or its photosynthetic pathway (C3 vs. C4) (e.g., Dorale, 1998; Partin et al., 2013), and in-cave CO_2 degassing and drip rate (Frisia et al., 2011; Mühlinghaus et al., 2007). Additionally, drip path controls directly linked to infiltrating rainfall amounts such as PCP and increased WRI in the epikarst can shift $\delta^{13}C$ more positive during dry periods (Fairchild et al., 2006; Johnson et al., 2006; Oster et al., 2010). Many of the potential $\delta^{13}C$ controls may work in tandem to create more positive $\delta^{13}C$ when conditions are locally dry (Wong & Breecker, 2015). However, $\delta^{13}C$ can also decrease during drier periods, as increased open-system dissolution will source more drip water carbon (and therefore speleothem carbon) from the organically fractionated soil-zone, which is significantly more negative

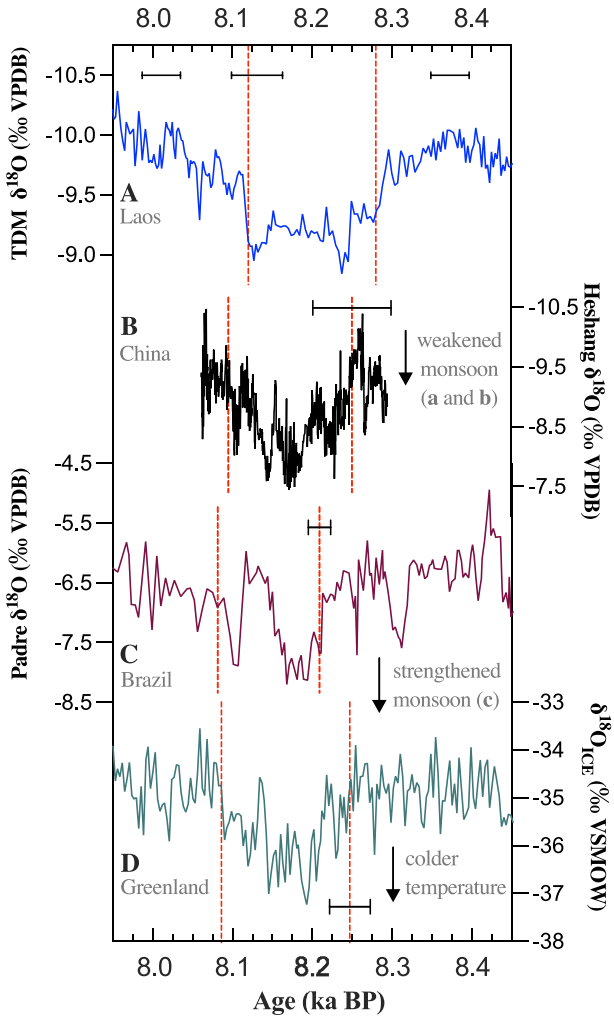

Figure 6. Selection of global 8.2 ka event $\delta^{18}O$ responses. (a) Stalagmite TM-17 from Tham Doun Mai (TDM), Northern Laos (this study). U-Th dates for plotted date range (n = 3) are shown as black brackets above data for TM-17. (b) HS4 stalagmite from Heshang Cave, China (Y. H. Liu et al., 2013) (c) PAD07 stalagmite from Padre Cave, Brazil (Cheng, Fleitmann, et al., 2009). (d) Composite, normalized record of isotopic data from four ice cores in Greenland (Thomas et al., 2007). Dashed vertical lines for each record display event beginning and end according to individual study criteria, and bracket on event initiation (b–d) represent the average approximate error for the respective record.

compared to a bedrock carbon source (Fohlmeister et al., 2011; Griffiths et al., 2012; Hendy, 1971; Oster et al., 2010).

TM-17 $\delta^{13}C$ decreases rapidly at the initiation of the 8.2 ka event (Figure 3). This initial decrease in $\delta^{13}C$ coincides with the onset of initially high Mg/Ca and Sr/Ca interpreted as an abrupt onset of drought conditions as well as a weakened monsoon state interpreted from TM-17 $\delta^{18}O$. Therefore, more negative values of $\delta^{13}C$ may be driven by increased open system dissolution due to drier conditions. In contrast to this control, increased PCP, WRI, and other non-dissolution controls active during dry conditions would enrich ^{13}C, opposing the open system dissolution control. The complex and at times opposing controls potentially explain the high variability and large swings in $\delta^{13}C$ during the event (Figure 3). The ambiguity of which $\delta^{13}C$ control is dominant, and for how long, creates uncertainty in $\delta^{13}C$ interpretations and in estimates of event length using this proxy alone. Additionally, the increased length of the event response in $\delta^{13}C$ (relative to $\delta^{18}O$), while discontinuous, is potentially attributable to local environmental controls that take longer to recover from the climatic disruption of the 8.2 ka event, such as changes in vegetation density and soil respiration.

Notably, $\delta^{13}C$ from TM-17 and other stalagmites from TDM cave show positive anomalies during drought conditions (Griffiths et al., 2020; J. K. Wang et al., 2019), suggesting that non-dissolution related controls are active for much of the Holocene. However, we suggest the 8.2 ka event response in TM-17 $\delta^{13}C$ is very likely dominated by increased open system dissolution for three reasons. First, the speleothems utilized in Griffiths et al. (2020) are from a different section of the cave that is situated below significantly thinner bedrock overburden than TM-17 (~20 vs. ~100 m, respectively) (Dreybrodt & Laumanns, 2013). An increase in overburden thickness may increase the degree of control open system dissolution would have on $\delta^{13}C$ due to drip water transit times and their exposure to open system conditions. Second, maximum shifts in more recent TM-17 $\delta^{13}C$ (up to 2 ka BP) are ~2‰ VDPB from average in either direction (J. K. Wang et al., 2019). At the 8.2 ka event, TM-17 $\delta^{13}C$ shifts ~2.63‰ more negatively than the pre-event average, and the total negative shift at the initial disruption is close to 4.00‰ (Figure 3). This relatively large shift suggests a greater proxy disruption at 8.2 ka BP compared to the most recent 2 ka BP. Third, and most importantly, the trace element proxies (Mg/Ca and Sr/Ca) show similar variations, which very likely indicates that PCP and/or WRI dominate those proxies, with drier conditions having higher X/Ca values. If PCP was the dominant control on $\delta^{13}C$, as is often the case (e.g., in Griffiths et al., 2020), then we would expect $\delta^{13}C$ to positively correlate with Mg/Ca and Sr/Ca, rather than display an antiphase relationship as is the case during the 8.2 ka event (Figure 3). Given that no other known mechanism could explain a negative $\delta^{13}C$ shift during a dry period (and vice-versa), we interpret the initial, negative shift in $\delta^{13}C$ as likely driven by an increase in open system dissolution due to drier conditions based on other TM-17 proxies: the more positive trend in $\delta^{18}O$ at this time indicating a weakened monsoon state and the highest values of Mg/Ca and Sr/Ca in the record at the same time as the large negative shift in $\delta^{13}C$ (Figure 3). The open system dissolution control active on $\delta^{13}C$ may not respond similarly or quickly enough to record the ~30 years reversal/period of wetter conditions seen in Mg/Ca and Sr/Ca following the initial disruption. These complex interpretations demonstrate the value of a multi-proxy approach to deconvolve potentially conflicting controls on speleothem carbon isotopes, as well as the potential for $\delta^{13}C$ controls to vary depending on timescale and cave setting.

TM-17 calcite fabric as observed in optical microscopy vary between compact columnar translucent calcite (Cc) and porous opaque calcite (Cp) layers (Frisia, 2015) (Figure 5b). Compact layers are usually indicative of constant and slow drip rates (dry periods), whereas porous fabrics are associated with higher and variable drip

rates which create macro (intercrystalline) and micro-scale (intracrystalline) porosity within the columnar calcite fabric (Faraji et al., 2022; Frisia et al., 2022). The fluorescence as observed in thin section is usually stimulated by a high concentration in humic acids (Sliwinski & Stoll, 2021) and is indicative of high flushing of organic matter from the soil during high rainfall/infiltration events. Fluorescence in speleothems can also influence the Sr incorporation, and high organic matter/fluorescence usually corresponds to low Sr concentration (Borsato et al., 2007; Vanghi et al., 2019). In fact, in TM-17, the lowest Sr values correspond to some of the highest fluorescence and lowest transmittance values recorded during the entire investigated period (Figure 5).

TM-17 growth rates, estimated between U-Th sampling depths using COPRA age model output, vary between ~13 and 71 μm/year, with an overall mean of 24 μm/year (Figure 3). The slowest growth rate (~13 μm/year) occurs between ~8.37 and 8.13 ka BP, which includes the majority of the 8.2 ka event (Figures 2 and 3). While growth rate is not always a reliable proxy for drip rates and associated $CaCO_3$ precipitation amounts, low growth rates during this interval are consistent with an interpretation of drying, cooler air temperatures, or a change in Ca^{2+} concentrations (e.g., Y. H. Liu et al., 2013) in response to the 8.2 ka event.

4.2. The 8.2 ka Event in MSEA: Timing, Structure, and Comparisons to Other Studies

The initial timing of the positive $\delta^{18}O$ ($>2\sigma$) anomaly in TM-17 at 8.29 ± 0.03 ka BP (using the largest uncertainty in the two U-Th dates bordering the event) is within error of published records of the 8.2 ka event onset around the world, including other speleothem records from Asia, Oman, and Brazil, as well as Greenland temperature proxy records from ice cores (Figure 6) (Cheng, Fleitmann, et al., 2009; Y. H. Liu et al., 2013; Thomas et al., 2007). The similarity in timing of 8.2 ka event responses in speleothem $\delta^{18}O$ in numerous global regions suggests teleconnections to an abrupt North Atlantic freshwater input are active on multiple continents and synchronous within age errors. Our data suggest MSEA responds similarly to previously documented Asian Monsoon locations that display a weakened monsoon state following the event initiation.

An onset of 8.25 ± 0.10 ka BP is estimated in Y. H. Liu et al. (2013), a stalagmite study from Heshang Cave, China (Figure 1f; 30°27′N, 110°25′E; 294 m asl) in which the relatively high growth rate of the sample allowed annual layer counting (annual layers of ~50–750 μm). A similar onset of 8.254 ± 0.03 ka BP is estimated using stalagmite data from North China (Duan et al., 2023). Greenland ice core age models utilizing annual layer counting (±50 years), display a similar start date (Figure 6) (Thomas et al., 2007), while stalagmites from multiple locations in the Asian and South American monsoons record $\delta^{18}O$ anomalies that collectively suggest the event response begins at 8.21 ± 0.02 ka BP (Cheng, Fleitmann, et al., 2009). TM-17 U-Th age uncertainties are often under 30 years (Table 1), and resolution in the COPRA age model approaches yearly at some points, but TM-17 does not possess visible yearly layers during the 8.2 ka event period. Additionally, the slowed growth rate estimated between ~8.37 and 8.13 ka BP (Figure 2) surrounding the event initiation could contain periods of uneven growth during changing environmental conditions. Thus, the estimate of 8.29 ± 0.03 ka BP from TM-17 $\delta^{18}O$, while within error of Duan et al. (2023) and Y. H. Liu et al. (2013), may not be as accurate as previous estimates that utilized annual layer counting.

Regardless of the exact initiation date, proxies in TM-17 sensitive to local hydrology indicate an event response decades earlier than an estimate using only $\delta^{18}O$ criteria. The initiation of a 2σ anomaly in TM-17 $\delta^{13}C$ and Mg/Ca occurs at 8.36 ± 0.03 ka BP (Figure 3), within the upper error of the Y. H. Liu et al. (2013) estimate from Heshang Cave, but up to ~70 years before the significant (2σ) anomaly begins in TM-17 $\delta^{18}O$. However, an increase in $\delta^{18}O$ ($<2\sigma$) begins at the time of both the Mg/Ca and $\delta^{13}C$ excursions, suggesting monsoon intensity may have begun weakening as decreases in local rainfall impacted other proxies. A long transport time for precipitation and/or mixing of water in the epikarst could create a lag in the initiation of the event as seen in $\delta^{18}O$ compared to Mg/Ca and $\delta^{13}C$, as hydrologic controls such as open system dissolution, PCP, and WRI could have a more immediate effect on epikarst drip water following a decrease in rainfall. Additionally, changes to regional atmospheric precipitation patterns that dictate the monsoon intensity signal might take longer to manifest following a global disruption in atmospheric circulation.

Interestingly, de Wet et al. (2021) propose a "precursor event" ~100 years prior to the 8.2 ka event based on a multiproxy speleothem record from California (de Wet et al., 2021; Oster et al., 2017). The timing of the precursor event (~8.3 ka BP), which results in a more sustained increase in precipitation in California than the event itself, is very similar to the timing of the initial Mg/Ca, Sr/Ca, $\delta^{13}C$, and fluorescence anomalies seen in TM-17.

de Wet et al. (2021) propose that the initial meltwater pulse may have altered North Pacific storm tracks prior to the manifestation of a global event response. Our trace element and fluorescence data suggest there may have been a similar period of increased rainfall and infiltration in MSEA before the initiation of the 8.2 ka event. This wet period follows an initial hydrologic disruption but precedes the long-term period of drier conditions during the event (Figure 4). $\delta^{13}C$ in TM-17 shows a strong shift at the start of the potential pre-event period synchronous with Mg/Ca and Sr/Ca, and we interpret this shift as an increase in open system dissolution due to dry conditions that matches the initial, sharp increase in LA-ICPMS Mg/Ca and Sr/Ca. However, there is not a similar reverse trend (more positive values of $\delta^{13}C$) synchronous with observed drops in Mg/Ca and Sr/Ca during the pre-event period (Figures 3 and 4). Instead, the suddenly more negative $\delta^{13}C$ trends slowly more positive with movement in both directions. These observations are potentially due to the opposing controls active on TM-17 $\delta^{13}C$ as well as the long recovery time for major changes in vegetation and soil dynamics that can affect speleothem $\delta^{13}C$. Calcite fabric and fluorescence changes in TM-17 are consistent along the studied period and corroborate the hydroclimate interpretation of the Mg/Ca and Sr/Ca (Figure 5). During the "precursor event" from ~8.36 to 8.33 ka BP, the highest fluorescence values are associated with the lowest Sr and optical transmittance values. This distinctive layer is characterized by high micro-porosity and dissolution features at the crystal tips suggesting fast infiltration events and, likely, organic matter oxidation. At the onset and during the 8.2 ka event, the fluorescence decreases to the minima levels, while the optical transmittance values are the highest of the entire studied interval (Figures 5b and 5e). Due to age uncertainties in both records and climatic differences between MSEA and Western North America, it is difficult to hypothesize that the precursor event period is connected or global in nature. However, this possibility could be explored with additional highly resolved and multiproxy records of the event from these and other regions.

Depending on the proxy and criteria applied, the length of the 8.2 ka event response in TM-17 proxies is similar to or longer than the ~150–160 years estimates of other studies (Cheng, Fleitmann, et al., 2009; Y. H. Liu et al., 2013; Thomas et al., 2007). The 2σ anomaly in TM-17 $\delta^{18}O$ data that lasts ~170 years is the most similar to previous studies (Figure 6). As our interpretation of $\delta^{18}O$ is not directly related to rainfall amounts, it follows that the event may have only affected the regional monsoon intensity signal for a time range similar to other event length estimates. TM-17 proxies more indicative of local water balance ($\delta^{13}C$ and Mg/Ca) indicate a longer local climate disruption, but a definitive length of the event response is less clear in these proxies (Figure 3). The ongoing period of discontinuous anomalies in Mg/Ca and $\delta^{13}C$, however, suggests that both are the result of locally dry or highly variable conditions that continue for decades or centuries after the event period as defined by $\delta^{18}O$.

In summary, the event response as defined by TM-17 proxy data lasts from ~170 years ($\delta^{18}O$ instrumental data using 2σ anomaly range) to a maximum of ~420 years ($\delta^{13}C$ discontinuous anomaly; Figure 3), although the maximum length suggests sustained hydrologic variability rather than an event period. Using $\delta^{13}C$ and Mg/Ca data for the initiation of the event and the 2σ anomaly in $\delta^{18}O$ instrumental data for the end of the event may offer the most confident estimate of event length using TM-17 multiproxy data, as $\delta^{13}C$ and Mg/Ca offer a similar onset but no specific end point. The event response using these criteria lasts for ~240 years (~8.36–8.12 ka BP; Figure 3). This may be a minimum length for the MSEA hydrological response, as the more positive trend in $\delta^{18}O$ begins prior to the 2σ anomaly. Additionally, after the initial hydrologic disruption, a relatively brief period of increased rainfall is suggested by TM-17 trace element proxies and fluorescence, suggesting a potential precursor event that could be separate from 8.2 ka event drying.

Some proxy records of the 8.2 ka event display evidence for a multi-stage event, which could be caused by separate drainage events from North American glacial lakes into the North Atlantic (Alley et al., 1997; Ellison et al., 2006; LeGrande & Schmidt, 2008; Rohling & Pälike, 2005; Teller et al., 2002). In the EASM domain, as well as monsoon records from Brazil and Madagascar, previously reported proxy data sometimes display a "double-plunging" structure that may indicate multiple stages of freshwater input (Figure 6) (Cheng, Fleitmann, et al., 2009; Duan et al., 2023; Voarintsoa et al., 2019). However, LeGrande and Schmidt (2008) find, using an ensemble isotope-enabled coupled atmosphere ocean climate model (GISS ModelE-R), that multiple meltwater stages are not required to create a multi-stage climate event, although they also cannot rule out the possibility. The TM-17 $\delta^{18}O$ record contains a comparable double-plunging structure as well a similar end-date (~8.12 ka BP) to the event response estimated utilizing several records in Cheng, Fleitmann, et al. (2009) (8.08 ka BP). Accounting for age uncertainties and potential shifts in growth rate for TM-17, the "plunging" structures could potentially line up with similar structures in other 8.2 ka event $\delta^{18}O$ records (Figure 6). However, TM-17 $\delta^{13}C$ and Mg/Ca do not mirror the exact timing or double-plunging structure of the $\delta^{18}O$ data, suggesting that any potential structural

similarity to other records is likely due to changes in monsoon intensity controls and not directly related to local rainfall amounts.

Model simulations have been successful in reproducing the 8.2 ka event in some respects, such as the overall patterns of global precipitation and temperature change (Morrill, Anderson, et al., 2013; Morrill, Legrande, Renssen, Bakker, & Otto-Bliesner, 2013). In reference to MSEA, these model simulations show modest and irregularly spaced drying. TM-17 proxy data (this study), in addition to recent $\delta^{18}O$ stalagmite records from Southern Thailand (Figure 1c) (Chawchai et al., 2021), expand the available records of speleothem-based 8.2 climatic responses in MSEA and provide evidence that the region experienced drying during the event. Comparing simulations to spatially widespread proxy records of the 8.2 event, Morrill, Legrande, Renssen, Bakker, and Otto-Bliesner (2013) also find that the patterns of global change often match in the direction of temperature and precipitation anomalies, though the duration of the event is typically too short. The timespan of anomalies in TM-17 proxies (minimum of ~170 years in $\delta^{18}O$; ~240+ years in other proxies) provides additional evidence that the event was both global and long-lived, supporting the need for previously proposed changes to 8.2 ka event model simulations such as a larger freshwater forcing, higher sensitivity of climate to freshwater inputs in the North Atlantic, and/or a weakened AMOC background state prior to the event (Morrill, Legrande, Renssen, Bakker, & Otto-Bliesner, 2013; Tindall & Valdes, 2011).

5. Conclusions

We present the first high-resolution, multiproxy speleothem study from MSEA that records how the 8.2 ka event affected both monsoon intensity and local hydrology in the understudied region connecting the ISM and the EASM. We interpret abrupt dryness and a weakened monsoon state following the event initiation, likely in response to a southward shifted ITCZ after a glacial outburst flood in the North Atlantic weakened the AMOC. This interpretation is in broad agreement with globally dispersed proxy records and model simulations (e.g., Cheng, Fleitmann, et al., 2009; Y. H. Liu et al., 2013; Morrill, Anderson, et al., 2013; Morrill, Legrande, et al., 2013; Thomas et al., 2007). Our record suggests MSEA monsoon strength and hydrology are affected by a climate teleconnection to the North Atlantic at least under abrupt and massive freshwater release. The event initiation date estimated from TM-17 $\delta^{18}O$ (8.29 ka BP $\pm$ 0.03) is within error of previous studies, and the minimum length for the local climatic response (~170 years in $\delta^{18}O$) aligns well with previously estimated lengths of a global scale event (~150–160 years) from sources such as Greenland ice cores and speleothem records from the EASM, Brazil, and Oman.

Multiproxy data from TM-17, however, reveal an earlier initiation for the event and enhance the climatic interpretations available from $\delta^{18}O$ alone, which typically documents large-scale monsoon intensity in speleothems from the Asian Monsoon domain. $\delta^{13}C$ and Mg/Ca data provide evidence for abrupt rainfall amount changes ~70 years prior to the start of the $\delta^{18}O$ anomaly, which extends the estimate of a total event response to at least ~240 years. These changes include a potential precursor period of increased rainfall lasting ~30 years prior to drier conditions that define for the majority of the event response. $\delta^{13}C$ and Mg/Ca data also display discontinuous excursions from each proxy's pre-event average that reach ~400 years or more in total. These hydroclimate observations may be specific to our study area, but a current lack of multiproxy, high resolution data in the greater monsoon region may prevent similar observations elsewhere on MSEA, in the EASM, and/or the ISM. Most currently available records of the event from these regions focus on speleothem $\delta^{18}O$ data or use archives, such as lake sediments, which are typically lower resolution and offer less precise age models. We emphasize the utility of multiproxy speleothem records for both climatological and chronological assessments of abrupt events in the paleoclimate record. Specifically, records of climatic change following the 8.2 ka event may assist in establishing the sensitivity of the climate to past freshwater inputs into the North Atlantic, which represent a potential analog for the future climate response to projected ice sheet melting.

Data Availability Statement

All speleothem (TM-17) proxy data sets and U-Th results utilized in this article are available at https://doi.org/10.25921/seqw-yh76 (Wood et al., 2023).

Acknowledgments
We thank Norseng Sayvongdouane (Traditional Fine Art College of Luang Prabang Province, Lao P.D.R.); Bounheuang Bouasisengpaseuth and other participants in the Middle Mekong Archaeology Project; and Lao government officials and departments for their assistance with the fieldwork, which was funded in part by Henry Luce Foundation grant to the University of Pennsylvania Museum. We thank two anonymous reviewers for their constructive suggestions that assisted in greatly improving the article. This work was supported by National Science Foundation P2C2 awards 1603056 and 1405472 to K.R.J., and National Science Foundation awards 1602947 and 1404932, and a William Paterson University Center for Research summer grant to M.L.G. ARCS Foundation Orange County provided support through an ARCS Scholar award to C.T.W. The SR-XRF analyses were undertaken at the X-ray fluorescence microscopy beamline at the Australian Synchrotron, Victoria, Australia under experiment 11048.

References

Allan, M., Fagel, N., van der Lubbe, H. J. L., Vonhof, H. B., Cheng, H., Edwards, R. L., & Verheyden, S. (2018). High-resolution reconstruction of 8.2-ka BP event documented in Père Noël cave, southern Belgium. *Journal of Quaternary Science*, *33*(7), 840–852. https://doi.org/10.1002/jqs.3064

Alley, R. B., & Ágústsdóttir, A. M. (2005). The 8k event: Cause and consequences of a major Holocene abrupt climate change. *Quaternary Science Reviews*, *24*(10–11), 1123–1149. https://doi.org/10.1016/j.quascirev.2004.12.004

Alley, R. B., Mayewski, P. A., Sowers, T., Stuiver, M., Taylor, K. C., & Clark, P. U. (1997). Holocene climatic instability: A prominent, widespread event 8200 yr ago. *Geology*, *25*(6), 483–486. https://doi.org/10.1130/0091-7613(1997)025<0483:HCIAPW>2.3.CO;2

Banerji, U. S., Arulbalaji, P., & Padmalal, D. (2020). Holocene climate variability and Indian Summer Monsoon: An overview. *The Holocene*, *30*(5), 744–773. https://doi.org/10.1177/0959683619895577

Berkelhammer, M., Sinha, A., Stott, L., Cheng, H., Pausata, F. S. R., & Yoshimura, K. (2012). An abrupt shift in the Indian monsoon 4000 years ago. *Geophysical Monograph Series*, *198*, 75–87. https://doi.org/10.1029/2012GM001207

Borsato, A., Frisia, S., Fairchild, I. J., Somogyi, A., & Susini, J. (2007). Trace element distribution in annual stalagmite laminae mapped by micrometer-resolution X-ray fluorescence: Implications for incorporation of environmentally significant species. *Geochimica et Cosmochimica Acta*, *71*(6), 1494–1512. https://doi.org/10.1016/j.gca.2006.12.016

Borsato, A., Frisia, S., Howard, D., & Greig, A. (2021). A guide to synchrotron hard X-ray fluorescence mapping of annually laminated stalagmites: Sample preparation, analysis and evaluation. *Spectrochimica Acta Part B: Atomic Spectroscopy*, *185*, 106308. https://doi.org/10.1016/j.sab.2021.106308

Bradley, C., Baker, A., Jex, C. N., & Leng, M. J. (2010). Hydrological uncertainties in the modelling of cave drip-water $\delta^{18}O$ and the implications for stalagmite palaeoclimate reconstructions. *Quaternary Science Reviews*, *29*(17–18), 2201–2214. https://doi.org/10.1016/j.quascirev.2010.05.017

Breitenbach, S. F. M., Rehfeld, K., Goswami, B., Baldini, J. U. L., Ridley, H. E., Kennett, D. J., et al. (2012). Constructing proxy records from age models (COPRA). *Climate of the Past*, *8*(5), 1765–1779. https://doi.org/10.5194/cp-8-1765-2012

Chabangborn, A., Punwong, P., Phountong, K., Nudnara, W., Yoojam, N., Sainakum, A., et al. (2020). Environmental changes on the west coast of the Gulf of Thailand during the 8.2 ka event. *Quaternary International*, *536*, 103–113. https://doi.org/10.1016/j.quaint.2019.12.020

Chawchai, S., Chabangborn, A., Kylander, M., Löwemark, L., Mörth, C. M., Blaauw, M., et al. (2013). Lake Kumphawapi—An archive of Holocene palaeoenvirontal and palaeoclimatic changes in northeast Thailand. *Quaternary Science Reviews*, *68*, 59–75. https://doi.org/10.1016/j.quascirev.2013.01.030

Chawchai, S., Tan, L., Löwemark, L., Wang, H. C., Yu, T. L., Chung, Y. C., et al. (2021). Hydroclimate variability of central Indo-Pacific region during the Holocene. *Quaternary Science Reviews*, *253*, 106779. https://doi.org/10.1016/j.quascirev.2020.106779

Cheng, H., Edwards, R. L., Broecker, W. S., Denton, G. H., Kong, X., Wang, Y., et al. (2009). Ice age terminations. *Science*, *326*(5950), 248–252. https://doi.org/10.1126/science.1177840

Cheng, H., Edwards, R. L., Shen, C. C., Polyak, V. J., Asmerom, Y., Woodhead, J., et al. (2013). Improvements in ^{230}Th dating, ^{230}Th and ^{234}U half-life values, and U-Th isotopic measurements by multi-collector inductively coupled plasma mass spectrometry. *Earth and Planetary Science Letters*, *371*(372), 82–91. https://doi.org/10.1016/j.epsl.2013.04.006

Cheng, H., Edwards, R. L., Sinha, A., Spötl, C., Yi, L., Chen, S., et al. (2016). The Asian monsoon over the past 640,000 years and ice age terminations. *Nature*, *534*(7609), 640–646. https://doi.org/10.1038/nature18591

Cheng, H., Fleitmann, D., Edwards, R. L., Wang, X., Cruz, F. W., Auler, A. S., et al. (2009). Timing and structure of the 8.2 kyr B.P. event inferred from $\delta^{18}O$ records of stalagmites from China, Oman, and Brazil. *Geology*, *37*(11), 1007–1010. https://doi.org/10.1130/G30126A.1

Chiang, J. C. H., Fung, I. Y., Wu, C. H., Cai, Y., Edman, J. P., Liu, Y., et al. (2015). Role of seasonal transitions and westerly jets in East Asian paleoclimate. *Quaternary Science Reviews*, *108*, 111–129. https://doi.org/10.1016/j.quascirev.2014.11.009

Dayem, K. E., Molnar, P., Battisti, D. S., & Roe, G. H. (2010). Lessons learned from oxygen isotopes in modern precipitation applied to interpretation of speleothem records of paleoclimate from eastern Asia. *Earth and Planetary Science Letters*, *295*(1–2), 219–230. https://doi.org/10.1016/j.epsl.2010.04.003

de Wet, C. B., Erhardt, A. M., Sharp, W. D., Marks, N. E., Bradbury, H. J., Turchyn, A. V., et al. (2021). Semiquantitative estimates of rainfall variability during the 8.2 kyr event in California using speleothem calcium isotope ratios. *Geophysical Research Letters*, *48*(3), 1–11. https://doi.org/10.1029/2020GL089154

Dixit, Y., Hodell, D. A., Sinha, R., & Petrie, C. A. (2014). Abrupt weakening of the Indian summer monsoon at 8.2 kyr B.P. *Earth and Planetary Science Letters*, *391*, 16–23. https://doi.org/10.1016/j.epsl.2014.01.026

Dong, J., Wang, Y., Cheng, H., Hardt, B., Lawrence Edwards, R., Kong, X., et al. (2010). A high-resolution stalagmite record of the Holocene East Asian monsoon from Mt Shennongjia, central China. *The Holocene*, *20*(2), 257–264. https://doi.org/10.1177/0959683609350393

Dorale, J. A. (1998). Climate and vegetation history of the midcontinent from 75 to 25 ka: A speleothem record from Crevice Cave, Missouri, USA. *Science*, *282*(5395), 1871–1874. https://doi.org/10.1126/science.282.5395.1871

Dreybrodt, J., & Laumanns, M. (Eds.). (2013). *The unknown north of Laos, Part 5—2012–2013: Karst and caves of the provinces Luang Nam Tha, Luang Prabang and Houaphan* (Vol. 49, pp. 5–148). Berliner Hoehlenkundliche Berichte.

Dreybrodt, J., Laumanns, M., & Steiner, H. (2013). Ten years of exploration and over 100 km of caves surveyed in Northern Laos. *UIS Congress Brno*, *2013*, 68–70.

Duan, P., Li, H., Ma, Z., Zhao, J., Dong, X., Sinha, A., et al. (2023). Interdecadal to centennial climate variability surrounding the 8.2 ka event in North China revealed through an annually resolved speleothem record from Beijing. *Geophysical Research Letters*, *50*(1), e2022GL101182. https://doi.org/10.1029/2022GL101182

Duan, P., Li, H., Sinha, A., Voarintsoa, N. R. G., Kathayat, G., Hu, P., et al. (2021). The timing and structure of the 8.2 ka event revealed through high-resolution speleothem records from northwestern Madagascar. *Quaternary Science Reviews*, *268*, 107104. https://doi.org/10.1016/j.quascirev.2021.107104

Dykoski, C. A., Edwards, R. L., Cheng, H., Yuan, D., Cai, Y., Zhang, M., et al. (2005). A high-resolution, absolute-dated Holocene and deglacial Asian monsoon record from Dongge Cave, China. *Earth and Planetary Science Letters*, *233*(1–2), 71–86. https://doi.org/10.1016/j.epsl.2005.01.036

Ellison, C. R. W., Chapman, M. R., & Hall, I. R. (2006). Surface and deep ocean interactions during the cold climate event 8200 years ago. *Science*, *312*(5782), 1929–1932. https://doi.org/10.1126/science.1127213

Fairchild, I. J., Smith, C. L., Baker, A., Fuller, L., Spötl, C., Mattey, D., et al. (2006). Modification and preservation of environmental signals in speleothems. *Earth-Science Reviews*, *75*(1–4), 105–153. https://doi.org/10.1016/j.earscirev.2005.08.003

Fairchild, I. J., & Treble, P. C. (2009). Trace elements in speleothems as recorders of environmental change. *Quaternary Science Reviews*, *28*(5–6), 449–468. https://doi.org/10.1016/j.quascirev.2008.11.007

Faraji, M., Borsato, A., Frisia, S., Mattey, D. P., Drysdale, R. N., Verdon-Kidd, D. C., et al. (2022). Controls on rainfall variability in the tropical South Pacific for the last 350 years reconstructed from oxygen isotopes in stalagmites from Cook Islands. *Quaternary Science Reviews*, *289*, 107633. https://doi.org/10.1016/j.quascirev.2022.107633

Feinberg, J. M., & Johnson, K. R. (2021). Cave and speleothem science: From local to planetary scales. *Elements*, *17*(2), 81–86. https://doi.org/10.2138/GSELEMENTS.17.2.81

Fohlmeister, J., Kromer, B., & Mangini, A. (2011). The influence of soil organic matter age spectrum on the reconstruction of atmospheric ^{14}C levels via stalagmites. *Radiocarbon*, *53*(1), 99–115. https://doi.org/10.1017/s003382220003438x

Frisia, S. (2015). Microstratigraphic logging of calcite fabrics in speleothems as tool for palaeoclimate studies. *International Journal of Speleology*, *44*(1), 1–16. https://doi.org/10.5038/1827-806X.44.1.1

Frisia, S., Borsato, A., Faraji, M., Hartland, A., Demeny, A., Drysdale, R., et al. (2022). Multi-step growth mechanisms in speleothems from the South Pacific and influences on climate proxy data. *Quaternary Science Reviews*, *297*, 107833. https://doi.org/10.1016/j.quascirev.2022.107833

Frisia, S., Fairchild, I. J., Fohlmeister, J., Miorandi, R., Spötl, C., & Borsato, A. (2011). Carbon mass-balance modelling and carbon isotope exchange processes in dynamic caves. *Geochimica et Cosmochimica Acta*, *75*(2), 380–400. https://doi.org/10.1016/j.gca.2010.10.021

Genty, D., Baker, A., Massault, M., Proctor, C., Gilmour, M., Pons-Branchu, E., & Hamelin, B. (2001). Dead carbon in stalagmites: Carbonate bedrock paleodissolution vs. ageing of soil organic matter. Implications for ^{13}C variations in speleothems. *Geochimica et Cosmochimica Acta*, *65*(20), 3443–3457. https://doi.org/10.1016/S0016-7037(01)00697-4

Griffiths, M. L., Fohlmeister, J., Drysdale, R. N., Hua, Q., Johnson, K. R., Hellstrom, J. C., et al. (2012). Hydrological control of the dead carbon fraction in a Holocene tropical speleothem. *Quaternary Geochronology*, *14*, 81–93. https://doi.org/10.1016/j.quageo.2012.04.001

Griffiths, M. L., Johnson, K. R., Pausata, F. S. R., White, J. C., Henderson, G. M., Wood, C. T., et al. (2020). End of Green Sahara amplified mid- to late Holocene megadroughts in mainland Southeast Asia. *Nature Communications*, *11*(1), 1–12. https://doi.org/10.1038/s41467-020-17927-6

Hendy, C. (1971). The isotopic geochemistry of speleothems—I. The calculation of the effects of different modes of formation on the isotopic composition of speleothems and their applicability as palaeoclimatic indicators. *Geochimica et Cosmochimica Acta*, *35*(8), 801–824. https://doi.org/10.1016/0016-7037(71)90127-X

Hu, C., Henderson, G. M., Huang, J., Xie, S., Sun, Y., & Johnson, K. R. (2008). Quantification of Holocene Asian monsoon rainfall from spatially separated cave records. *Earth and Planetary Science Letters*, *266*(3–4), 221–232. https://doi.org/10.1016/j.epsl.2007.10.015

Johnson, K. R. (2011). Palaeoclimate: Long-distance relationship. *Nature Geoscience*, *4*(7), 426–427. https://doi.org/10.1038/ngeo1190

Johnson, K. R. (2021a). California's volatile hydroclimate: Lessons from the paleoclimate record. *Geophysical Research Letters*, *48*(23), 1–6. https://doi.org/10.1029/2021GL095512

Johnson, K. R. (2021b). Tales from the underground: Speleothem records of past hydroclimate. *Elements*, *17*(2), 93–100. https://doi.org/10.2138/gselements.17.2.93

Johnson, K. R., Hu, C., Belshaw, N. S., & Henderson, G. M. (2006). Seasonal trace-element and stable-isotope variations in a Chinese speleothem: The potential for high-resolution paleomonsoon reconstruction. *Earth and Planetary Science Letters*, *244*(1–2), 394–407. https://doi.org/10.1016/j.epsl.2006.01.064

Kiernan, K. (2015). Karst geomorphology along the Nam Ou, northern Lao PDR. *Cave and Karst Science*, *42*(2), 86–94.

Kleiven, H. F., Kissel, C., Laj, C., Ninnemann, U. S., Richter, T. O., & Cortijo, E. (2008). Reduced North Atlantic deep water coeval with the glacial lake Agassiz freshwater outburst. *Science*, *319*(5859), 60–64. https://doi.org/10.1126/science.1148924

Kobashi, T., Severinghaus, J. P., Brook, E. J., Barnola, J.-M., & Grachev, A. M. (2007). Precise timing and characterization of abrupt climate change 8200 years ago from air trapped in polar ice. *Quaternary Science Reviews*, *26*(9–10), 1212–1222. https://doi.org/10.1016/J.QUASCIREV.2007.01.009

LeGrande, A. N., & Schmidt, G. A. (2008). Ensemble, water isotope-enabled, coupled general circulation modeling insights into the 8.2 ka event. *Paleoceanography*, *23*(3), PA3207. https://doi.org/10.1029/2008PA001610

Liu, G., Li, X., Chiang, H. W., Cheng, H., Yuan, S., Chawchai, S., et al. (2020). On the glacial-interglacial variability of the Asian monsoon in speleothem $\delta^{18}O$ records. *Science Advances*, *6*(7), 1–11. https://doi.org/10.1126/sciadv.aay8189

Liu, Y. H., Henderson, G. M., Hu, C. Y., Mason, A. J., Charnley, N., Johnson, K. R., & Xie, S. C. (2013). Links between the East Asian monsoon and North Atlantic climate during the 8,200 year event. *Nature Geoscience*, *6*(2), 117–120. https://doi.org/10.1038/ngeo1708

Ljung, K., Björck, S., Renssen, H., & Hammarlund, D. (2008). South Atlantic island record reveals a South Atlantic response to the 8.2 kyr event. Retrieved from https://hal.archives-ouvertes.fr/hal-00298102/

Mason, A. J., & Henderson, G. M. (2010). Correction of multi-collector-ICP-MS instrumental biases in high-precision uranium-thorium chronology. *International Journal of Mass Spectrometry*, *295*(1–2), 26–35. https://doi.org/10.1016/j.ijms.2010.06.016

Matero, I. S. O., Gregoire, L. J., Ivanovic, R. F., Tindall, J. C., & Haywood, A. M. (2017). The 8.2 ka cooling event caused by Laurentide ice saddle collapse. *Earth and Planetary Science Letters*, *473*, 205–214. https://doi.org/10.1016/J.EPSL.2017.06.011

Maxwell, A. L. (2001). Holocene monsoon changes inferred from lake sediment pollen and carbonate records, northeastern Cambodia. *Quaternary Research*, *56*(3), 390–400. https://doi.org/10.1006/qres.2001.2271

McManus, J. F., Francois, R., Gheraradi, J. M., Keigwin, L. D., & Brown-Leger, S. (2004). Collapse and rapid resumption of Atlantic meridional circulation linked to glacial climate changes. *Nature*, *428*, 834–837. https://doi.org/10.1038/nature02494

Morrill, C., Anderson, D. M., Bauer, B. A., Buckner, R., Gille, E. P., Gross, W. S., et al. (2013). Proxy benchmarks for intercomparison of 8.2 ka simulations. *Climate of the Past*, *9*(1), 423–432. https://doi.org/10.5194/cp-9-423-2013

Morrill, C., & Jacobsen, R. M. (2005). How widespread were climate anomalies 8200 years ago? *Geophysical Research Letters*, *32*(19), 1–4. https://doi.org/10.1029/2005GL023536

Morrill, C., Legrande, A. N., Renssen, H., Bakker, P., & Otto-Bliesner, B. L. (2013). Model sensitivity to North Atlantic freshwater forcing at 8.2 ka. *Climate of the Past*, *9*(2), 955–968. https://doi.org/10.5194/cp-9-955-2013

Morrill, C., Wagner, A., Otto-Bliesner, B., & Rosenbloom, N. (2011). Evidence for significant climate impacts in monsoonal Asia at 8.2 ka from multiple proxies and model simulations. *Journal of Earth Environment*, *2*(3), 426–441. http://nldr.library.ucar.edu/repository/collections/OSGC-000-000-003-851

Mühlinghaus, C., Scholz, D., & Mangini, A. (2007). Modelling stalagmite growth and $\delta^{13}C$ as a function of drip interval and temperature. *Geochimica et Cosmochimica Acta*, *71*(11), 2780–2790. https://doi.org/10.1016/j.gca.2007.03.018

Oster, J. L., Montañez, I. P., Guilderson, T. P., Sharp, W. D., & Banner, J. L. (2010). Modeling speleothem $\delta^{13}C$ variability in a central Sierra Nevada cave using ^{14}C and $^{87}Sr/^{86}Sr$. *Geochimica et Cosmochimica Acta*, *74*(18), 5228–5242. https://doi.org/10.1016/j.gca.2010.06.030

Oster, J. L., Sharp, W. D., Covey, A. K., Gibson, J., Rogers, B., & Mix, H. (2017). Climate response to the 8.2 ka event in coastal California. *Scientific Reports*, *7*(1), 1–9. https://doi.org/10.1038/s41598-017-04215-5

Owen, R. A., Day, C. C., Hu, C. Y., Liu, Y. H., Pointing, M. D., Blättler, C. L., & Henderson, G. M. (2016). Calcium isotopes in caves as a proxy for aridity: Modern calibration and application to the 8.2 kyr event. *Earth and Planetary Science Letters*, *443*, 129–138. https://doi.org/10.1016/j.epsl.2016.03.027

Partin, J. W., Cobb, K. M., Adkins, J. F., Tuen, A. A., & Clark, B. (2013). Trace metal and carbon isotopic variations in cave dripwater and stalagmite geochemistry from northern Borneo. *Geochemistry, Geophysics, Geosystems*, *14*(9), 3567–3585. https://doi.org/10.1002/ggge.20215

Paton, C., Hellstrom, J., Paul, B., Woodhead, J., & Hergt, J. (2011). Iolite: Freeware for the visualisation and processing of mass spectrometric data. *Journal of Analytical Atomic Spectrometry*, *26*(12), 2508–2518. https://doi.org/10.1039/C1A10172B

Patterson, E. W., Johnson, K. R., Griffiths, M. L., Kinsley, C. W., McGee, D., Du, X., et al. (2023). Glacial changes in sea level modulated millennial-scale variability of Southeast Asian autumn monsoon rainfall. *Proceedings of the National Academy of Sciences*, *120*(27), e2219489120. https://doi.org/10.1073/pnas

Pausata, F. S. R., Battisti, D. S., Nisancioglu, K. H., & Bitz, C. M. (2011). Chinese stalagmite $\delta^{18}O$ controlled by changes in the Indian monsoon during a simulated Heinrich event. *Nature Geoscience*, *4*(7), 474–480. https://doi.org/10.1038/ngeo1169

Peros, M., Collins, S., G'Meiner, A. A., Reinhardt, E., & Pupo, F. M. (2017). Multistage 8.2 kyr event revealed through high-resolution XRF core scanning of Cuban sinkhole sediments. *Geophysical Research Letters*, *44*(14), 7374–7381. https://doi.org/10.1002/2017GL074369

Rohling, E., & Pälike, H. (2005). Centennial-scale climate cooling with a sudden cold event around 8,200 years ago. *Nature*, *434*(7036), 975–979. https://doi.org/10.1038/nature03421

Ryan, W. B. F., Carbotte, S. M., Coplan, J. O., O'Hara, S., Melkonian, A., Arko, R., et al. (2009). Global multi-resolution topography synthesis. *Geochemistry, Geophysics, Geosystems*, *10*(3), Q03014. https://doi.org/10.1029/2008GC002332

Sinclair, D. J., Banner, J. L., Taylor, F. W., Partin, J., Jenson, J., Mylroie, J., et al. (2012). Magnesium and strontium systematics in tropical speleothems from the Western Pacific. *Chemical Geology*, *294–295*, 1–17. https://doi.org/10.1016/j.chemgeo.2011.10.008

Sliwinski, J. T., & Stoll, H. M. (2021). Combined fluorescence imaging and LA-ICPMS trace element mapping of stalagmites: Microfabric identification and interpretation. *Chemical Geology*, *581*, 120397. https://doi.org/10.1016/j.chemgeo.2021.120397

Teller, J. T., Leverington, D. W., & Mann, J. D. (2002). Freshwater outbursts to the oceans from glacial Lake Agassiz and their role in climate change during the last deglaciation. *Quaternary Science Reviews*, *21*(8–9), 879–887. https://doi.org/10.1016/S0277-3791(01)00145-7

Thomas, E. R., Wolff, E. W., Mulvaney, R., Steffensen, J. P., Johnsen, S. J., Arrowsmith, C., et al. (2007). The 8.2 ka event from Greenland ice cores. *Quaternary Science Reviews*, *26*(1–2), 70–81. https://doi.org/10.1016/J.QUASCIREV.2006.07.017

Tindall, J. C., & Valdes, P. J. (2011). Modeling the 8.2 ka event using a coupled atmosphere–ocean GCM. *Global and Planetary Change*, *79*(3–4), 312–321. https://doi.org/10.1016/J.GLOPLACHA.2011.02.004

Treble, P. C., Baker, A., Abram, N. J., Hellstrom, J. C., Crawford, J., Gagan, M. K., et al. (2022). Ubiquitous karst hydrological control on speleothem oxygen isotope variability in a global study. *Communications Earth & Environment*, *3*(1), 29. https://doi.org/10.1038/s43247-022-00347-3

Tremaine, D. M., & Froelich, P. N. (2013). Speleothem trace element signatures: A hydrologic geochemical study of modern cave dripwaters and farmed calcite. *Geochimica et Cosmochimica Acta*, *121*, 522–545. https://doi.org/10.1016/j.gca.2013.07.026

Vanghi, V., Borsato, A., Frisia, S., Drysdale, R., Hellstrom, J., & Bajo, P. (2018). Climate variability on the Adriatic seaboard during the last glacial inception and MIS 5c from Frasassi cave stalagmite record. *Quaternary Science Reviews*, *201*, 349–361. https://doi.org/10.1016/j.quascirev.2018.10.023

Vanghi, V., Borsato, A., Frisia, S., Howard, D. L., Gloy, G., Hellstrom, J., & Bajo, P. (2019). High-resolution synchrotron X-ray fluorescence investigation of calcite coralloid speleothems: Elemental incorporation and their potential as environmental archives. *Sedimentology*, *66*(7), 2661–2685. https://doi.org/10.1111/sed.12607

Voarintsoa, N. R. G., Matero, I. S. O., Railsback, L. B., Gregoire, L. J., Tindall, J., Sime, L., et al. (2019). Investigating the 8.2 ka event in northwestern Madagascar: Insight from data–model comparisons. *Quaternary Science Reviews*, *204*, 172–186. https://doi.org/10.1016/j.quascirev.2018.11.030

Walker, M., Head, M. J., Berkelhammer, M., Björck, S., Cheng, H., Cwynar, L., et al. (2018). Formal ratification of the subdivision of the Holocene Series/Epoch (Quaternary System/Period): Two new Global Boundary Stratotype Sections and Points (GSSPs) and three new stages/subseries. *Episodes*, *41*(4), 213–223. https://doi.org/10.18814/epiiugs/2018/018016

Waltgenbach, S., Scholz, D., Spötl, C., Riechelmann, D. F. C., Jochum, K. P., Fohlmeister, J., & Schröder-Ritzrau, A. (2020). Climate and structure of the 8.2 ka event reconstructed from three speleothems from Germany. *Global and Planetary Change*, *193*, 103266. https://doi.org/10.1016/j.gloplacha.2020.103266

Wang, J. K., Johnson, K. R., Borsato, A., Amaya, D. J., Griffiths, M. L., Henderson, G. M., et al. (2019). Hydroclimatic variability in Southeast Asia over the past two millennia. *Earth and Planetary Science Letters*, *525*, 115737. https://doi.org/10.1016/j.epsl.2019.115737

Wang, Y. J., Cheng, H., Edwards, R. L., An, Z. S., Wu, J. Y., Shen, C. C., & Dorale, J. A. (2001). A high-resolution absolute-dated late Pleistocene Monsoon record from Hulu Cave, China. *Science*, *294*(5550), 2345–2348. https://doi.org/10.1126/science.1064618

Wang, Y. J., Cheng, H., Edwards, R. L., He, Y., Kong, X., An, Z., et al. (2005). The Holocene Asian monsoon: Links to solar changes and North Atlantic climate, *308*, 854–858.

Wendt, K. A., Li, X., & Edwards, R. L. (2021). Uranium-thorium dating of speleothems. *Elements*, *17*(2), 87–92. https://doi.org/10.2138/GSELEMENTS.17.2.87

Wong, C. I., & Breecker, D. O. (2015). Advancements in the use of speleothems as climate archives. *Quaternary Science Reviews*, *127*, 1–18. https://doi.org/10.1016/j.quascirev.2015.07.019

Wood, C. T., Johnson, K. R., Lewis, L. E., Wright, K. T., Wang, J. K., Borsato, A., et al. (2023). NOAA/WDS Paleoclimatology—Tham Doun Mai Cave, Northern Laos Trace Metal and Stable Isotope Data from 7.6 to 9 ka [Dataset]. NOAA National Centers for Environmental Information. https://doi.org/10.25921/seqw-yh76

Wright, K. T., Johnson, K. R., Marks, G. S., McGee, D., Bhattacharya, T., Goldsmith, G. R., et al. (2023). Dynamic and thermodynamic influences on precipitation in Northeast Mexico on orbital to millennial timescales. *Nature Communications*, *14*(1), 2279. https://doi.org/10.1038/s41467-023-37700-9

Yang, H., Johnson, K. R., Griffiths, M. L., & Yoshimura, K. (2016). Interannual controls on oxygen isotope variability in Asian monsoon precipitation and implications for paleoclimate reconstructions. *Journal of Geophysical Research: Atmospheres*, *121*(14), 8410–8428. https://doi.org/10.1002/2015JD024683

Yuan, D., Cheng, H., Edwards, R. L., Dykoski, C. A., Kelly, M. J., Zhang, M., et al. (2004). Timing, duration, and transitions of the last interglacial Asian Monsoon. *Science*, *304*(5670), 575–578. https://doi.org/10.1126/science.1091220

Zhang, H., Griffiths, M. L., Chiang, J. C. H., Kong, W., Wu, S., Atwood, A., et al. (2018). East Asian hydroclimate modulated by the position of the westerlies during Termination I. *Science*, *362*(6414), 580–583. https://doi.org/10.1126/science.aat9393